CTNND1 (p120-Catenin; Catenin Delta-1), VAV3, and Network Entropy as Candidate Biomarkers of Gefitinib Resistance in Non-Small Cell Lung Cancer

Dimitra C. Tsakona and Nikolaos A. Papanikolaou *

Posted Date: 25 March 2026

doi: 10.20944/preprints202603.1918.v1

Keywords: NSCLC; gefitinib resistance; network entropy; protein interaction networks; CTNND1; VAV3; EGFR; Rho-GTPase; systems biology; small-world networks

 doi:10.20944/preprints202603.1918.v1

Article

CTNND1 (p120-Catenin; Catenin Delta-1), VAV3, and Network Entropy as Candidate Biomarkers of Gefitinib Resistance in Non-Small Cell Lung Cancer

Dimitra C. Tsakona [1] and Nikolaos A. Papanikolaou [2,3,*]

[1] Department of Biology, Inter-Faculty Program on Networks and Complexity, Aristotle University of Thessaloniki, Thessaloniki 54124, Greece

[2] Department of Basic Sciences, Touro College of Osteopathic Medicine, Touro University, New York USA

[3] Laboratory of Biological Chemistry, Aristotle University of Thessaloniki School of Medicine, Thessaloniki, Macedonia, Greece

* Correspondence: npapanik@touro.edu

Abstract

Acquired resistance to EGFR tyrosine kinase inhibitors remains a principal barrier to durable remission in non-small cell lung cancer (NSCLC). Using a time-resolved protein interaction network analysis of isogenic Gefitinib-sensitive and resistant NSCLC cells, we show that network entropy increases progressively under drug treatment in both phenotypes, while small-world topology is lost, consistent with Gefitinib's dismantling of EGFR-centered signaling hubs. Eigenvector entropy alone distinguished the resistant phenotype at baseline, reflecting a pre-established, robustly buffered network state. Co-expression network analysis revealed a resistance-specific subnetwork in which delta-catenin (CTNND1) serves as the dominant topological bridge between EGFR, VAV3, HIF3A, and NOTCH2, four nodes independently linked to chemoresistance but not previously connected within a single regulatory network. We propose that HIF1α-driven induction of CTNND1, EGFR-mediated positive feedback, and VAV3-dependent Rho-GTPase activation cooperate to drive actin cytoskeletal remodeling and phenotypic switching. BIRC3 emerged as an independent late-stage apoptotic block exclusive to resistant cells. These findings nominate CTNND1 and VAV3 as candidate co-targets and eigenvector entropy as a systems-level biomarker of Gefitinib resistance.

Keywords: NSCLC; gefitinib resistance; network entropy; protein interaction networks; CTNND1; VAV3; EGFR; Rho-GTPase; systems biology; small-world networks

1. Introduction

Non-small cell lung cancer (NSCLC) represents more than 80% of all lung cancer diagnoses worldwide and carries a five-year survival rate below 15% [1,2]. Among NSCLC patients, activating mutations in the epidermal growth factor receptor (EGFR), principally exon 19 deletions and the exon 21 L858R substitution, which together account for approximately 85% of all sensitizing EGFR mutations — confer susceptibility to EGFR-tyrosine kinase inhibitors (EGFR-TKIs) such as Gefitinib [3,4]. Despite pronounced initial clinical responses, most patients develop acquired resistance. Approximately 60% of first-generation EGFR-TKI resistance cases are attributed to the secondary T790M gatekeeper mutation; second- and third-generation inhibitors have partially addressed this, but secondary resistance mechanisms involving C797S, L718Q, and L792H mutations, bypass signaling, epithelial-to-mesenchymal transition (EMT), and transcriptomic reprogramming continue to limit durable clinical benefit [5–8].

A defining feature of cancer is the high degree of cellular plasticity it confers, the capacity to adopt alternative signaling states in response to genetic, epigenetic, or pharmacological perturbations [9–14]. From a systems biology perspective, the functional state of a cell can be represented as a

 doi:10.20944/preprints202603.1918.v1

protein interaction network (PIN), in which nodes are proteins and edges are validated physical interactions. Aberrant cellular states, including drug resistance, can therefore be conceptualized as topological and entropic changes in these networks: alterations in the network's nodes and edges may reflect, at the systems level, the phenotypic consequences of individual molecular perturbations [15–17].

Network entropy, a measure of the diversification or randomness of local interaction patterns within a PIN, has emerged as a biologically meaningful quantifier of cellular state. West et al. demonstrated that PIN entropy is significantly elevated in cancer cells relative to matched normal tissue [18]. Banerji et al. showed that entropy scales with differentiation potential across multiple lineages, with embryonic stem cells exhibiting the highest values [19]. Breitkreutz et al. reported a correlation between PIN entropy and five-year survival in cancer patients [20,24–26]. Mechanistic support for these observations derives from the entropy-robustness theorem of Demetrius et al. [21], which formalizes the positive correlation between a system's macroscopic resilience R and its microscopic network entropy S, expressed as $\Delta S \Delta R < 0$: as robustness increases, entropy increases proportionately. This framework predicts that drug-resistant cancer cells, which are by definition more robust, should exhibit higher network entropy than sensitive counterparts.

Despite these advances, the dynamic evolution of PIN entropy under sustained chemotherapy, and its relationship to the acquisition of drug resistance, has not been characterized in a time-resolved manner. Here we address this gap. We hypothesized that while network entropy would increase in both phenotypes under drug pressure, the entropy profiles of sensitive and resistant cells would differ in ways that reflect the distinct robustness of the resistant phenotype, and that network centrality analysis would identify candidate molecular drivers of resistance. Using publicly available time-course microarray data (GEO: GSE34228) from isogenic Gefitinib-sensitive PC9 and Gefitinib-resistant PC9R NSCLC cells, we constructed and analyzed DEG-derived PINs at five time points across 24 hours of Gefitinib administration.

Our main findings are: (i) entropy of all measured local network properties increases over 24 hours in both phenotypes; (ii) small-world topology is progressively lost in both cell lines; (iii) eigenvector entropy uniquely discriminates resistant from sensitive cells at the pre-treatment (1h) baseline; (iv) BIRC3 is the dominant hub protein in resistant cells at 24h, absent from the sensitive network; and (v) co-expression network analysis identifies a resistance-specific subnetwork centered on delta-catenin (CTNND1), connecting EGFR, VAV3, NOTCH2, and HIF3A, from which we derive a testable mechanistic model of Gefitinib resistance.

2. Materials and Methods

2.1. Dataset

Gene expression data from Gefitinib-sensitive (PC9) and Gefitinib-resistant (PC9R) NSCLC cells were retrieved from the NCBI Gene Expression Omnibus (accession: GSE34228). This publicly available dataset, generated by Nakata et al., comprises normalized time-course microarray measurements at five time points (1h, 6h, 12h, 18h, 24h) following Gefitinib treatment, in paired untreated controls for both cell lines. All analyses were performed on publicly available, fully anonymized data; no new patient-derived or animal samples were used.

2.2. Differential Expression Analysis

Differential expression between Gefitinib-treated and untreated cells were quantified using the limma package in R/Bioconductor following GEO2R default settings. For each gene *i*, the $\log_2$-transformed fold change ($\log_2$FC) was computed at each time point. Significance was assessed by the Benjamini–Hochberg false discovery rate (FDR) correction, with an adjusted p-value (adj-P) threshold of 0.05. Genes were ranked by $|\log_2 FC|$ in descending order, and the top 1,000 significant DEGs per cell line per time point were used for temporal PIN construction. For co-expression network analysis, all significant DEGs across the full 24-hour window were retained.

 doi:10.20944/preprints202603.1918.v1

Note on analytical assumption: this analysis assumes that significantly overexpressed genes are translated into functionally active proteins. Post-transcriptional and post-translational regulation may decouple mRNA levels from protein activity; this constitutes a recognized limitation of transcript-based PIN construction and is discussed further in Section 4.5.

2.3. Construction of Temporal Protein Interaction Networks

For each combination of cell line and time point, significant DEGs were submitted as queries to STRINGdb v11 [22] with the organism parameter set to Homo sapiens. Only experimentally validated protein-protein interactions (physical binding, as curated from primary literature) were retained; interactions inferred from co-expression, text-mining, or computational prediction were excluded. This yielded ten temporal PINs (5 time points × 2 cell lines). Network construction was performed in Python using the NetworkX library.

2.4. Construction of Co-Expression-Augmented Protein Interaction Networks

Two co-expression-augmented PINs were constructed to broaden the regulatory context. The seed gene set for each cell line comprised: (i) the 100 top-ranked DEGs from GEO2R analysis; (ii) 100 significant genes from Gene Set Enrichment Analysis (GSEA, default settings); and (iii) 300 genes co-expressed with EGFR in the COEXPRESS database (EGFR as query, default settings). STRING dB experimentally validated interactions among these 500 seed genes were retrieved for each cell line, yielding two co-expression PINs.

2.5. Network Analysis

For each PIN, the following global properties were computed: order (number of nodes), size (number of edges), graph density, number of connected components, giant component (GC) order and size, diameter, average path length, global and local clustering coefficients (transitivity), assortativity, degree/betweenness/closeness centralization, and small-world index. The small-world index was computed as

$$\sigma = \frac{\left(\frac{C}{Crand}\right)}{\left(\frac{L}{Lrand}\right)}$$

where C and L are the observed clustering coefficient and average path length respectively, and the subscripted values are the corresponding parameters for a size-matched Erdős–Rényi random graph; a value > 1 is required for small-world classification [23]. Degree distributions were fitted to power-law models using the power law package; goodness-of-fit was assessed by the Kolmogorov–Smirnov p-value, with $p > 0.05$ indicating compatibility with a power-law distribution.

Five network entropy metrics were computed as the Shannon entropy H of normalized node-property distributions: degree entropy, betweenness entropy, closeness entropy, eigenvector entropy, and clustering entropy. Entropy values were normalized to [0,1] except in cases of highly heterogeneous degree distributions where normalization is undefined. Nodes with the maximum value of each centrality measure at each time point were identified and annotated using UniProt and the Gene Ontology database.

3. Results

3.1. Differential Gene Expression After Gefitinib Administration

Gefitinib-sensitive PC9 and Gefitinib-resistant PC9R cells both showed robust and bidirectional differential gene expression at each time point (Supplementary Figures S1 and S2). Volcano plots confirmed substantial differential expression signals, and median-centered boxplot distributions confirmed inter-sample normalization quality. Limma-based filtering (adj-P < 0.05) yielded variable

 doi:10.20944/preprints202603.1918.v1

numbers of significant DEGs at individual time points across both cell lines. Across the full 24-hour treatment window used for co-expression PIN construction, PC9 cells yielded 19,995 significant DEGs and PC9R cells 16,776, providing a rich input for downstream network analysis.

3.2. Global Topology of Temporal PINs Is Scale-Free, Sparse, and Assortative

Temporal PINs for both cell lines were sparse (density ≤ 0.022 at all time points), disconnected (containing 19–50 components), and exhibited degree distributions compatible with power-law fits at most time points (KS $p > 0.05$; scaling exponents $\alpha \approx 1.7–3.8$), consistent with scale-free topology. All networks were assortative at every time point, indicating that highly connected proteins preferentially interact with each other. Selected global property values for sensitive and resistant cell networks are reported in Tables 1 and 2; complete properties are provided in Supplementary Tables S1 and S2.

Table 1. Global network properties of Gefitinib-sensitive PC9 temporal PINs.

Measure	1h	6h	12h	18h	24h
Order (nodes)	221	118	206	124	164
Size (edges)	478	140	358	150	128
No. of components	19	31	32	30	50
GC order	162	30	124	35	20
GC size	404	30	304	82	24
GC (% of total)	73%	25%	60%	28%	12%
Avg. path length	4.296	3.331	8.616	3.267	2.609
Graph density	0.019	0.020	0.016	0.019	0.009
Assortativity	0.441	0.695	0.597	0.562	0.270
Small-world index	5.157	0.048	0.626	0.578	0.231
Degree entropy	0.835	0.247	2.185	0.993	0.596
Betweenness entropy	0.601	0.774	0.765	0.857	0.899
Closeness entropy	0.945	0.668	0.708	0.845	0.868
Eigenvector entropy	0.457	0.963	0.937	0.985	0.984
Clustering entropy	0.659	0.963	0.438	0.915	0.994

GC = giant component. Bold values (small-world index ≥ 1) indicate networks retaining small-world topology. Entropy values are Shannon entropy of the respective normalized node-property distribution (range 0–1; degree entropy at 12h is unnormalized due to highly heterogeneous distribution). Complete network properties are provided in Supplementary Table S1.

Table 2. Global network properties of Gefitinib-resistant PC9R temporal PINs.

Measure	1h	6h	12h	18h	24h
Order (nodes)	138	218	168	134	128
Size (edges)	200	543	308	158	119

 doi:10.20944/preprints202603.1918.v1

No. of components	23	32	34	31	39
GC order	72	129	53	28	18
GC size	151	475	201	73	18
GC (% of total)	52%	59%	32%	21%	14%
Avg. path length	6.215	6.337	3.488	2.952	2.672
Graph density	0.021	0.022	0.021	0.017	0.014
Assortativity	0.625	0.408	0.518	0.587	0.502
Small-world index	2.030	1.703	0.981	0.906	0.337
Degree entropy	0.806	0.799	0.887	0.895	0.931
Betweenness entropy	0.683	0.641	0.804	0.801	0.825
Closeness entropy	0.954	0.953	0.980	0.968	0.968
Eigenvector entropy	0.503	0.647	0.905	0.944	0.987
Clustering entropy	0.551	0.714	0.795	0.758	0.507

See Table 1 for notation. Complete network properties are provided in Supplementary Table S2.

3.3. Progressive Network Fragmentation Under Sustained Gefitinib Treatment

PC9 PINs exhibited progressive reduction in order, size, and giant component (GC) across the 24-hour treatment period (Tables 1 and 2; Figure 1). In PC9R cells, network parameters showed an initial expansion at 6h (order: 138 → 218; edges: 200 → 543; GC: 52% → 59%), followed by progressive fragmentation from 12h onward, suggesting an early compensatory rewiring response absent from sensitive cells. In PC9 cells, the GC declined from 73% of total nodes at 1h to 12% at 24h; in PC9R cells, from 52% to 14% (Figure 1). This fragmentation reflects the loss of connectivity among the most drug-responsive proteins under sustained EGFR pathway suppression. Importantly, although both cell lines showed fragmentation, the PC9 sensitive network fragmented more severely by the 24h endpoint, whereas the resistant PC9R network maintained more connectivity through 6h (GC = 59% at 6h), consistent with greater early resilience in the resistant phenotype.

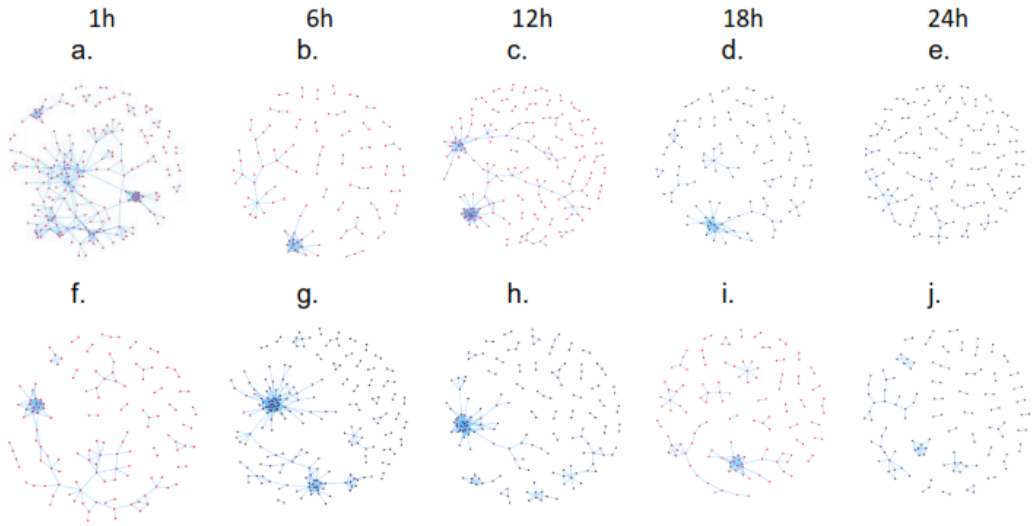

 doi:10.20944/preprints202603.1918.v1

Figure 1. Protein interaction networks of differentially expressed genes in Gefitinib-sensitive PC9 cells (a–e) and Gefitinib-resistant PC9R cells (f–j) at five time points (1h, 6h, 12h, 18h, 24h) after Gefitinib administration. Progressive reduction of the giant component reflects network rewiring under sustained EGFR pathway suppression.

3.4. Network Entropy Trajectories Under Gefitinib Treatment: General Upward Trend in Both Phenotypes

Entropy of all five local network measures (degree, betweenness, closeness, eigenvector, and clustering) showed a progressively upward trend over the 24-hour treatment period in both PC9 and PC9R cells (Tables 1 and 2; Figure 2). The highest entropy values were generally observed at 18h and 24h.relative to 1h and 6h, indicating progressive diversification of interaction patterns under sustained drug pressure. This universal trend is consistent with the entropy-robustness theorem: Gefitinib constitutes an external perturbation that forces both phenotypes toward higher-entropy network states (Figure 2).

a.

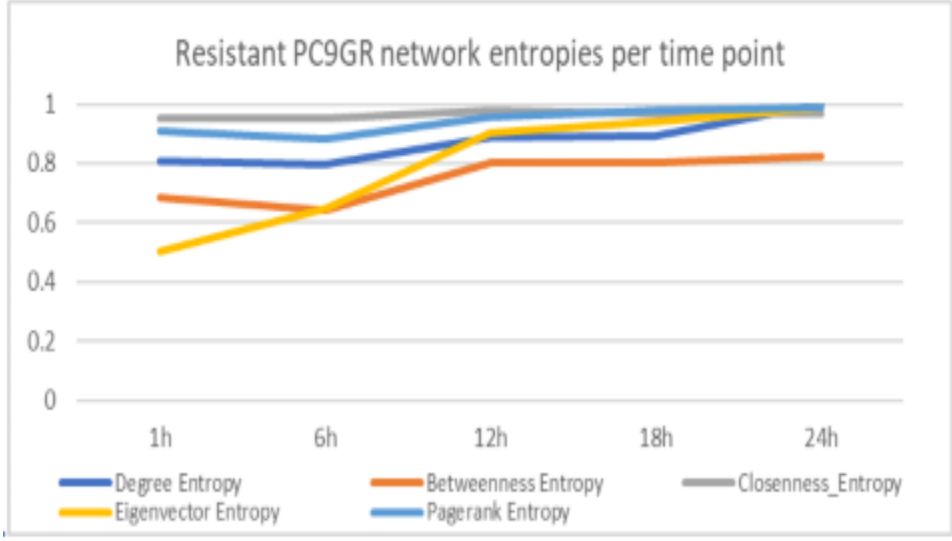

b.

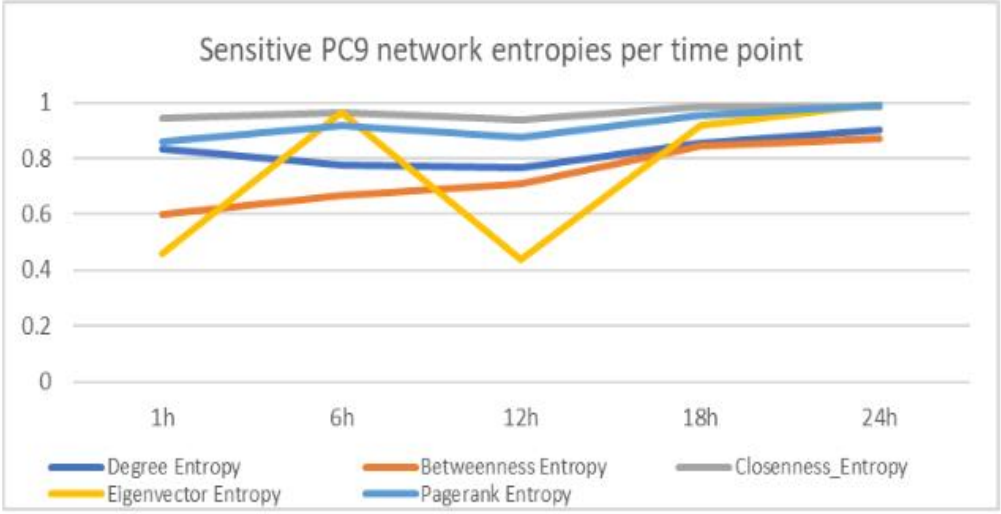

 doi:10.20944/preprints202603.1918.v1

Figure 2. Network entropy trajectories of local network properties in Gefitinib-resistant PC9R cells (a) and Gefitinib-sensitive PC9 cells (b) at five time points under Gefitinib treatment. All entropy measures increase over the 24-hour treatment course in both phenotypes. Eigenvector entropy (orange) shows the greatest baseline difference between phenotypes at 1h.

However, a critical distinction emerges when the two phenotypes are compared directly. Eigenvector entropy, which measures how uniformly regulatory influence is distributed across network nodes, was already elevated in PC9R resistant cells at the 1h baseline (0.503) compared to PC9 sensitive cells (0.457). By 24h both converge near 0.985 (Table 1) and 0.987 (Table 2), but the pre-existing elevation in resistant cells suggests a higher baseline network robustness consistent with a more undifferentiated, pluripotent-like signaling state, as predicted by the entropy-robustness framework [21] and supported by Banerji et al.'s work on differentiation potential [19]. This makes eigenvector entropy the only measure capable of distinguishing the two phenotypes, and a candidate pre-treatment biomarker of resistance. The temporal entropy trajectories for all measures in both cell lines are shown in Figure 2.

3.5. Progressive Loss of Small-World Topology

At 1h, both the PC9 (small-world index 5.157) and PC9R (2.030) networks possessed clear small-world properties (index > 1), characterized by high clustering relative to average path length. Small-world properties were lost earlier in sensitive cells (at 6h, index = 0.048) than in resistant cells (at 12h, index = 0.981); by 24h both had indices well below 1 (PC9: 0.231; PC9R: 0.337). This structural change is mechanistically coherent: Gefitinib inhibits EGFR autophosphorylation by competing with ATP at the tyrosine kinase domain, thereby dismantling the tightly clustered, EGFR-centered signaling modules that define small-world topology. The earlier and more abrupt loss of small-world properties in sensitive cells is consistent with their more complete and rapid suppression of EGFR signaling; resistant cells, by contrast, retain partial EGFR activity, possibly through T790M mutation or bypass mechanisms, which sustains clustered signaling modules for longer.

3.6. Key Hub and Bottleneck Proteins in Temporal Networks Reveal Phenotype-Specific Regulators

Proteins with maximum centrality values were identified at each time point in both cell lines (Table 3). In PC9 sensitive cells, prominent hub proteins over the treatment course included CREBBP (1h; chromatin remodeling), CDK1 (6h; G1/S cell cycle transition), MYC (12h; proliferation, apoptosis), CDC6 (18h; DNA replication licensing), and RRM2 (24h; nucleotide synthesis). The progressive shift from chromatin remodeling factors to DNA synthesis machinery suggests an ordered transcriptional response to EGFR inhibition in sensitive cells.

In PC9R resistant cells, the centrality landscape differed substantially. NOP56 (1h–6h; rRNA processing), CDC6 (12h), and EXO1 (18h; DNA repair and replication) dominated at early-to-mid time points. At 24h, BIRC3, a Baculoviral IAP Repeat Containing 3 protein and direct inhibitor of caspase-3, -7, and -9, became the single highest-centrality node across all four centrality measures (degree, betweenness, closeness, and eigenvector) in the resistant network, while being entirely absent from the highest-centrality positions in the sensitive network. BIRC3 has been associated with poor overall survival in NSCLC [27] and with chemoresistance in colorectal cancer [28,29]. Its emergence as the dominant network hub exclusively in resistant cells at 24h positions it as a candidate late-stage anti-apoptotic effector of Gefitinib resistance.

Table 3. Genes with maximum centrality at each time point in Gefitinib-sensitive PC9 and Gefitinib-resistant PC9R cells.

Centrality	1h	6h	12h	18h	24h
SENSITIVE PC9 cells					

 doi:10.20944/preprints202603.1918.v1

Degree	CREBBP	CDK1	EXO1	CDC6	RRM2
Betweenness	HIST1H2BJ	ABL1	MYC	PKMYT1	RRM2
Closeness	HIST1H2BJ	ABL1	MYC	PKMYT1	DTL
Eigenvector	VPRBP	CDK1	RRM2	CDC6	RRM2
RESISTANT PC9R cells					
Degree	NOP56	NOP56	CDC6	EXO1	BIRC3
Betweenness	ABL1	UBE2D1	PKMYT1	MCM10	BIRC3
Closeness	ABL1	WDR4	CDC6	MCM10	BIRC3
Eigenvector	NOP56	MRTO4	CDC6	EXO1	CASP10

Cells sharing the same gene at a given time point and centrality measure indicate convergence of topological importance. BIRC3 uniquely dominates all four centrality measures at 24h in resistant cells.

3.7. Co-Expression Network Analysis Identifies Resistance-Specific Bottleneck Nodes

Co-expression-augmented PINs were constructed for PC9 and PC9R cells to provide broader regulatory context. Global topological properties were broadly comparable between the two networks (Table 4; Supplementary Figure S3), both exhibiting small-world properties (PC9: 3.180; PC9R: 2.632), positive assortativity, and low density. These global similarities confirm that the two networks are structurally matched at a systems level, making local centrality differences more meaningful.

Table 4. Global properties of co-expression-augmented PINs for PC9 and PC9R cells.

Property	PC9 (Sensitive)	PC9R (Resistant)
Order (nodes)	138	116
Size (edges)	257	179
Density	0.0393	0.0376
Assortativity	0.204	0.086
Diameter	13	13
Small-world index	3.180	2.632
Degree entropy	0.816	0.783
Betweenness entropy	0.623	0.631
Closeness entropy	0.944	0.954
Eigenvector entropy	0.854	0.835
PageRank entropy	0.889	0.889
Clustering entropy	0.696	0.659

Notably, eigenvector entropy is modestly higher in PC9 sensitive cells in the co-expression PINs, in contrast to the resistant-higher pattern observed in the temporal PINs at 1h; this discrepancy may reflect the different gene set composition and network construction approach and warrants further investigation.

 doi:10.20944/preprints202603.1918.v1

Despite comparable global properties, the composition of the top 10 betweenness-centrality (bottleneck) nodes differed markedly. The PC9R resistant network uniquely contained VAV3 (Vav Guanine Nucleotide Exchange Factor 3), HIF3A (Hypoxia-Inducible Factor 3α), NOTCH2, and CITED2 as bottleneck nodes, all absent from the PC9 sensitive network (Figure 3). Additionally, delta-catenin (CTNND1) was the top betweenness-centrality node in the resistant co-expression network, acting topologically as a bridge connecting EGFR, VAV3, NOTCH2, and HIF3A within the same subnetwork. RhoV (Rho-related GTP-binding protein) appeared as an interactor of VAV3 exclusively in the resistant network. These findings delineate a resistance-specific molecular subnetwork and form the basis for the mechanistic model developed in the Discussion (Figure 3). Complete co-expression network properties are provided in Supplementary Table S3.

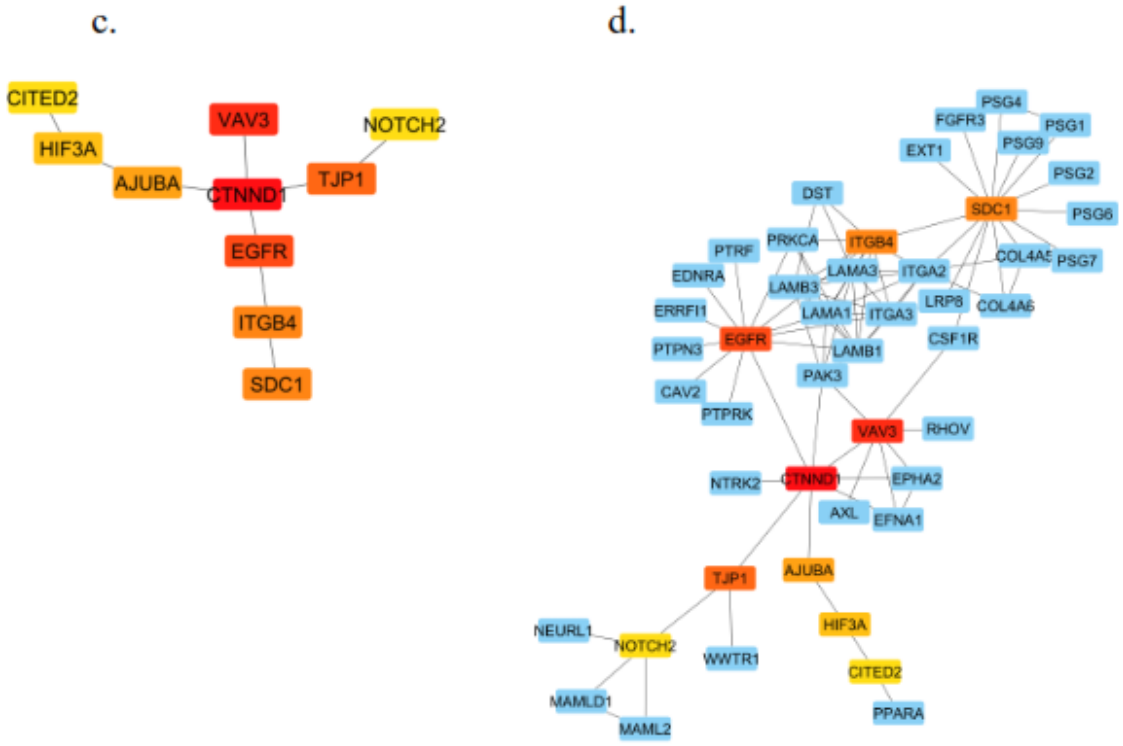

Figure 3. Resistance-specific co-expression subnetwork in Gefitinib-resistant PC9R cells. (c) The top 10 betweenness-centrality (bottleneck) nodes of the PC9R resistant network, with CTNND1 (δ-catenin, highlighted) as the dominant bridge node. (d) First-order interactors of the top 10 bottlenecks, revealing the EGFR–CTNND1–VAV3–NOTCH2–HIF3A connectivity. Nodes absent from the Gefitinib-sensitive PC9 bottleneck network include VAV3, HIF3A, NOTCH2, CITED2, and RhoV.

4. Discussion

4.1. Overview of Main Findings

This study provides the first time-resolved, systems-level characterization of PIN entropy and topology in NSCLC cells under Gefitinib treatment, comparing isogenic sensitive and resistant phenotypes across five time points. Five principal findings emerge. First, network entropy increases in both phenotypes under drug pressure, consistent with the entropy-robustness theorem. Second, small-world topology is progressively lost in both cell lines, consistent with the disruption of EGFR-anchored signaling hubs. Third, eigenvector entropy is the only measure to distinguish resistant from sensitive cells at baseline. Fourth, the co-expression analysis reveals a resistance-specific subnetwork centered on delta-catenin (CTNND1). Fifth, BIRC3 serves as a late-stage anti-apoptotic hub exclusively in resistant temporal networks.

 doi:10.20944/preprints202603.1918.v1

4.2. Network Entropy Increase as a Universal Response to Gefitinib

The progressive increase in all five entropy measures in both phenotypes is consistent with established observations that pharmacological perturbations increase the diversification of local interaction patterns in cancer PINs [18,30]. The loss of small-world properties is mechanistically coherent: Gefitinib inhibits EGFR autophosphorylation by blocking ATP binding to the tyrosine kinase domain, thereby disabling the central hub around which clustered signaling modules are organized. Disrupting such hubs in scale-free networks is well known to degrade small-world properties by fragmenting hub-mediated inter-cluster communication [31].

That entropy increases universally in both phenotypes reveals a fundamental limitation of the original thesis hypothesis — that drug resistance would be straightforwardly associated with higher PIN entropy than sensitivity. The data show instead that both phenotypes undergo entropic increases under drug pressure; resistance cannot be read off from entropy trajectories alone. Rather, it is the pre-existing baseline state and the specific topological differences (centrality landscape, co-expression subnetwork composition) that distinguish the resistant phenotype. This nuance is critical for the correct interpretation of network entropy as a resistance descriptor and for the design of future studies.

4.3. Eigenvector Entropy as a Candidate Marker of the Resistant State

Eigenvector entropy captures the extent to which regulatory influence is uniformly distributed across all network nodes, rather than concentrated in a small number of central hubs. A higher eigenvector entropy therefore reflects a more democratically connected network, in which many nodes contribute non-negligibly to overall network regulation, a property associated with higher robustness to targeted perturbations [19,21]. The higher baseline eigenvector entropy in PC9R cells (0.503 at 1h vs. 0.457 in PC9) is consistent with the more undifferentiated, pluripotent-like cellular state described for drug-resistant cancer cells by Banerji et al. [19], and with the view that resistant cells maintain a more broadly buffered, redundant signaling architecture.

The clinical implication is significant: if eigenvector entropy can be computed from a patient's tumor biopsy-derived transcriptomic data before treatment initiation, it may serve as a pre-treatment predictor of EGFR-TKI response. This hypothesis is directly testable using existing pan-cancer transcriptomic cohorts such as TCGA-LUAD, in which matched pre- and post-treatment samples are available. We propose this as a priority for follow-up work.

4.4. Resistance-Specific Hub Proteins: BIRC3 and UBE2D1

The emergence of BIRC3 as the dominant hub across all centrality measures in the resistant network at 24h is among the most biologically compelling findings of this study. BIRC3 belongs to the inhibitor of apoptosis (IAP) protein family and directly suppresses caspase-3, -7, and -9 activation through its BIR domains [32,33]. In NSCLC, higher BIRC3 expression has been independently associated with poorer overall survival [27]. In colorectal and hepatocellular cancers, BIRC3 upregulation has been linked to chemoresistance through inhibition of 5-FU-induced apoptosis, promotion of EMT, and facilitation of metastasis [28,29,34]. Our network analysis positions BIRC3 as a late-stage (24h) central regulatory node in the resistant cell's response to Gefitinib, suggesting it may actively suppress drug-induced apoptosis at the point when sensitive cells have committed to cell death. This warrants experimental validation: BIRC3 knockdown in PC9R cells under Gefitinib treatment should re-sensitize cells to apoptosis, a testable prediction.

At 6h in resistant cells, UBE2D1 (Ubiquitin Conjugating Enzyme E2 D1) held the highest betweenness centrality. UBE2D1 participates in the ubiquitination and proteasomal degradation of both the tumor suppressor p53 and the hypoxia-inducible transcription factor HIF1α, through its interaction with E3 ubiquitin-protein ligases including MDM2 [35]. As an early-time-point bottleneck exclusively in the resistant network, UBE2D1 may represent an early-phase ubiquitin-mediated resistance mechanism, potentially stabilizing HIF1α and thereby activating the hypoxia-related

 doi:10.20944/preprints202603.1918.v1

resistance nodes identified in the co-expression analysis. This positions UBE2D1 as a potential upstream enabler of the HIF3A-containing resistance subnetwork.

4.5. A Proposed EGFR/Notch/VAV3/HIF Axis Mediated by Delta-Catenin in Gefitinib-Resistant NSCLC

The most novel contribution of this study is the delineation of a resistance-specific co-expression subnetwork in which delta-catenin (CTNND1) serves as the topological hub connecting EGFR, VAV3, HIF3A, and NOTCH2, all proteins with independent evidence linking them to NSCLC chemoresistance, but whose mutual interactions in a single regulatory network have not previously been described.

The mechanistic plausibility of this subnetwork rests on three converging lines of evidence. First, **the EGFR–delta-catenin connection:** EGFR phosphorylates delta-catenin, enhancing EGFR signaling in a positive feedback loop [36]. Second, **the HIF–delta-catenin–Wnt axis:** HIF1α directly induces *Ctnnd1* expression [37], and delta-catenin stabilizes β-catenin by disrupting the destruction complex, thereby activating Wnt signaling. Third, **delta-catenin–Rho-GTPase coupling:** delta-catenin (and the broader p120-catenin family) regulates Rho-family GTPase activity, inhibiting RhoA and activating Rac1/Cdc42, thereby modulating actin cytoskeletal dynamics and cell motility [38,39].

VAV3, identified here as a resistance-specific bottleneck, is a guanine nucleotide exchange factor (GEF) that activates Rho-family GTPases by catalyzing GDP-to-GTP exchange [40]. It has been functionally linked to endocrine therapy resistance in breast cancer [41], to drug resistance in gastric cancer through MAPK/PI3K/AKT pathway modulation following VAV3 siRNA inhibition [42], and to tumor initiation through extracellular signaling loops [53]. In NSCLC, the role of VAV3 in EGFR-TKI resistance is unexplored; our network finding provides the first topological evidence for its involvement and suggests that VAV3 may amplify delta-catenin-mediated Rho-GTPase activation in the resistant state.

NOTCH2, the third resistance-specific bottleneck, has a well-established role in NSCLC survival, stemness, and EGFR-TKI resistance [43–46]. Critically, Notch signaling is required to maintain the undifferentiated cell state under hypoxia [47], and hypoxia has been linked to Gefitinib resistance through upregulation of FGFR1/MAPK [48] and TGFα/EGFR axes [49]. HIF3A, the fourth resistance-specific bottleneck, has been detected at aberrantly elevated levels in plasma and tumor tissue of NSCLC patients, where its expression may reflect active hypoxic responses [50].

Integrating these observations, we propose the following mechanistic model for the CTNND1-centered resistance subnetwork (Figure 4): hypoxia within the tumor microenvironment stabilizes HIF1α, which directly induces delta-catenin (CTNND1) expression. EGFR, which remains active at a baseline level in resistant cells despite Gefitinib treatment (possibly due to T790M mutation or alternative activation), phosphorylates delta-catenin, amplifying both EGFR and Wnt signaling. Delta-catenin, in concert with VAV3-mediated Rho-GTPase activation, promotes actin cytoskeletal remodeling, EMT, and survival signaling. NOTCH2, maintained in an active state by hypoxia via the HIF/Notch axis, further sustains stemness and resistance. This model is schematically testable: (i) CTNND1 knockdown in PC9R cells under Gefitinib should reduce VAV3-dependent Rho-GTPase activation and restore Gefitinib sensitivity; (ii) dual inhibition of EGFR and VAV3 (or CTNND1) should synergistically overcome resistance; (iii) HIF3A expression in patient biopsies should correlate with EGFR-TKI resistance status.

 doi:10.20944/preprints202603.1918.v1

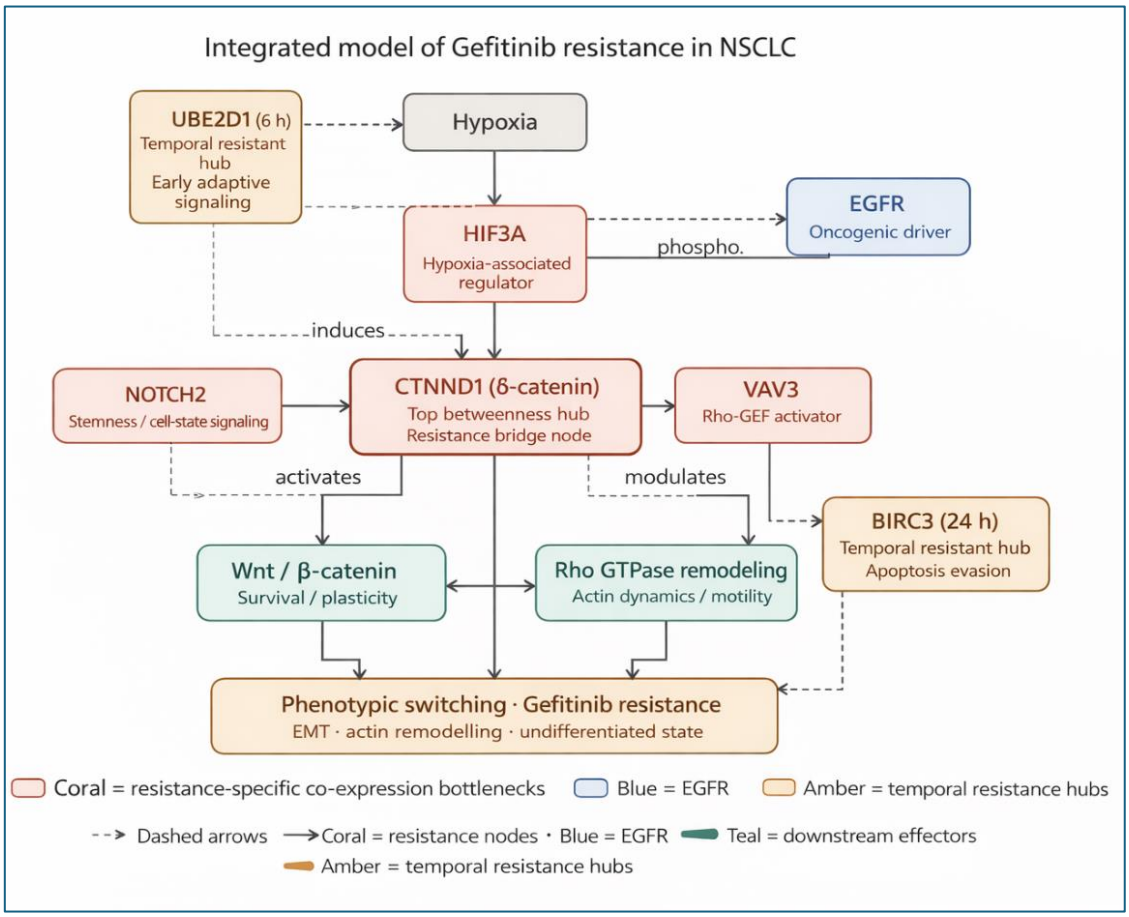

Figure 4. Integrated two-layer resistance model in Gefitinib-resistant NSCLC. A co-expression-derived resistance core centered on CTNND1 (δ-catenin) links HIF3A, NOTCH2, EGFR, and VAV3 to downstream survival signaling and cytoskeletal remodeling, culminating in phenotypic switching, epithelial-mesenchymal transition, and sustained Gefitinib resistance. To distinguish this layer from the temporal network analysis, UBE2D1 and BIRC3 are shown separately as early and late temporal resistant hubs, respectively, representing adaptive stress signaling and apoptosis evasion. Solid arrows denote core evidence-supported activating or inductive relationships, whereas dashed arrows denote temporal or hypothesized links.

4.6. Network Fragmentation and the 'Survival of the Sparsest' Principle

The progressive reduction in giant component size reflects network rewiring under sustained Gefitinib exposure. Studies on the evolution of gene regulatory networks suggest that selection favors sparse networks with minimal connectivity when the topology is free to evolve, the 'survival of the sparsest' principle [51]. In the context of Gefitinib treatment, the fragmentation of the initially connected DEG subnetwork may reflect the progressive disengagement of non-essential signaling modules, leaving only the most critical regulatory interactions intact. The retention of a more connected early-phase network in resistant cells (GC = 59% at 6h vs. 25% in sensitive cells) may reflect the greater modularity and redundancy of their signaling architecture, consistent with higher robustness [52].

4.7. Limitations and Future Directions

Several important limitations must be acknowledged. The use of the top 1,000 DEGs per time point as a fixed threshold is methodologically arbitrary. This choice was pragmatic but is not data-driven; a sensitivity analysis varying this threshold would strengthen the conclusions. The central analytical assumption, that significantly differentially expressed transcripts are translated into functionally active proteins, may be violated by post-transcriptional silencing, miRNA-mediated regulation, protein degradation, or localization-dependent inactivation. Future studies integrating

 doi:10.20944/preprints202603.1918.v1

proteomic or phosphoproteomic data with transcriptomic inputs would significantly improve network fidelity.

The co-expression network construction combined gene sets from three heterogeneous sources (GEO analysis, GSEA, COEXPRESS), which may introduce biases related to database coverage, platform differences, and experimental conditions. A more homogeneous, biologically motivated seed gene selection strategy would reduce this heterogeneity. Additionally, the study is based on two cell lines (PC9 and PC9R) and a single public dataset. While these are established isogenic models for EGFR-TKI sensitivity, the generalizability of the findings to patient tumors, which are genetically heterogeneous and embedded in a complex tumor microenvironment, requires validation.

Most fundamentally, the entire mechanistic model described in Section 4.5 is grounded in network topology and literature co-citation; it has not been experimentally validated. Functional experiments including co-immunoprecipitation (CTNND1 with EGFR, VAV3, NOTCH2), proximity ligation assays, CTNND1/VAV3 siRNA knockdown with Gefitinib sensitivity assays, and patient-cohort correlation analyses (eigenvector entropy with treatment outcome) are required to establish whether the proposed CTNND1-centered subnetwork is causally relevant to Gefitinib resistance rather than correlatively associated.

5. Conclusions

This study provides a time-resolved, systems-level characterization of protein interaction network entropy and topology in isogenic Gefitinib-sensitive and resistant NSCLC cells. Our five key findings are: (1) entropy of all measured local network properties increases progressively under Gefitinib treatment in both phenotypes, consistent with the entropy-robustness theorem; (2) small-world network properties are progressively lost in both cell lines, consistent with Gefitinib's disruption of EGFR-centered signaling hubs; (3) eigenvector entropy is the only entropy measure to distinguish the resistant from the sensitive phenotype at baseline, and is proposed as a candidate pre-treatment resistance biomarker; (4) BIRC3 emerges as the uniquely dominant hub protein in resistant cell networks at 24h, implicating anti-apoptotic resistance as a late-stage mechanism; and (5) co-expression network analysis identifies delta-catenin (CTNND1) as the top bottleneck in the resistant network, bridging EGFR, VAV3, NOTCH2, and HIF3A, from which a testable mechanistic model of Gefitinib resistance is derived. Delta-catenin and VAV3 are nominated as priority candidates for experimental validation and potential therapeutic co-targeting in Gefitinib-resistant NSCLC.

Supplementary Materials: The following supporting information can be downloaded at the website of this paper posted on Preprints.org.

Author Contributions: D.C.T.: Conceptualization, data acquisition and curation, differential expression analysis, network construction, network analysis, data interpretation, writing, original draft. N.A.P.: Supervision, conceptualization, data interpretation, writing, review and editing. All authors approved the final version of the manuscript.

Data Availability: The gene expression dataset analyzed in this study is publicly available in the NCBI Gene Expression Omnibus (GEO; https://www.ncbi.nlm.nih.gov/geo/) under accession number GSE34228. Network construction scripts are available from the corresponding author upon reasonable request. Supplementary Information is available for this article and includes Supplementary Methods, Supplementary Figures S1–S3, and Supplementary Tables S1–S3.

References

1. Sung H, et al. Global Cancer Statistics 2020: GLOBOCAN estimates. CA Cancer J Clin. 2021;71:209–249.
2. Miller KD, et al. Cancer treatment and survivorship statistics, 2019. CA Cancer J Clin. 2019;69:363–385.
3. Gazdar AF. Activating and resistance mutations of EGFR in NSCLC. Oncogene. 2009;28(Suppl 1):S24–31.
4. Ahsan A. Mechanisms of resistance to EGFR TKIs. Adv Exp Med Biol. 2016;893:137–153.

 doi:10.20944/preprints202603.1918.v1

5. Yun C-H, et al. The T790M mutation in EGFR kinase causes drug resistance by increasing ATP affinity. PNAS. 2008;105:2070–2075.
6. Thress KS, et al. Acquired EGFR C797S mutation mediates resistance to AZD9291 in NSCLC. Nat Med. 2015;21:560–562.
7. Chen Z, et al. Non-small-cell lung cancers: a heterogeneous set of diseases. Nat Rev Cancer. 2014;14:535–546.
8. Rotow J, Bivona TG. Understanding and targeting resistance mechanisms in NSCLC. Nat Rev Cancer. 2017;17:637–658.
9. Califano A. Rewiring makes the difference. Mol Syst Biol. 2011;7:463.
10. Dutkowski J, Ideker T. Protein networks as logic functions in development and cancer. PLoS Comput Biol. 2011;7:e1002180.
11. Creixell P, et al. Navigating cancer network attractors for tumor-specific therapy. Nat Biotechnol. 2012;30:842–848.
12. Pisco AO, et al. Non-Darwinian dynamics in therapy-induced cancer drug resistance. Nat Commun. 2013;4:2467.
13. Ideker T, Krogan NJ. Differential network biology. Mol Syst Biol. 2012;8:565.
14. Pawson T, Linding R. Network medicine. FEBS Lett. 2008;582:1266–1270.
15. Schlessinger J. Ligand-induced, receptor-mediated dimerization and activation of EGF receptor. Cell. 2002;110:669–672.
16. Garrett JT, Arteaga CL. Resistance to HER2-directed antibodies and TKIs. Cancer Biol Ther. 2011;11:793–800.
17. Al-Lazikani B, et al. Combinatorial drug therapy for cancer in the post-genomic era. Nat Biotechnol. 2012;30:679–692.
18. West J, et al. Differential network entropy reveals cancer system hallmarks. Sci Rep. 2012;2:802.
19. Banerji CRS, et al. Cellular network entropy as the energy potential in Waddington's differentiation landscape. Sci Rep. 2013;3:3039.
20. Breitkreutz D, et al. Molecular signaling network complexity correlates with cancer patient survivability. PNAS. 2012;109:9209–9212.
21. Demetrius L, et al. Complexity and demographic stability in population models. Theor Popul Biol. 2004;65:211–225.
22. Szklarczyk D, et al. STRING v11: protein–protein association networks with increased coverage. Nucleic Acids Res. 2019;47:D607–D613.
23. Walsh T. Search in a small world. IJCAI. 1999:1172–1177.
24. Teschendorff AE, Severini S. Increased entropy of signal transduction in the cancer metastasis phenotype. BMC Syst Biol. 2010;4:104.
25. Manke T, Demetrius L, Vingron M. Lethality and entropy of protein interaction networks. Genome Inform. 2005;16:153–163.
26. Teschendorff AE, Sollich P, Kuehn R. Signaling entropy: a network-theoretical framework for systems analysis of functional omic data. Methods. 2014;67:282–293.
27. Tang D, et al. Genetic variants of BIRC3 in the NLRP3 inflammasome pathway are associated with NSCLC survival. Am J Cancer Res. 2020;10:2582–2595.
28. Karasawa H, et al. Down-regulation of cIAP2 enhances 5-FU sensitivity in human colon cancer cells. Cancer Sci. 2009;100:903–913.
29. Krajewska M, et al. Analysis of apoptosis protein expression in early-stage colorectal cancer. Clin Cancer Res. 2005;11:5451–5461.
30. Ferrell JE. Tripping the switch fantastic: protein kinase cascades converting graded inputs into switch-like outputs. Trends Biochem Sci. 1996;21:460–466.
31. Barabási A-L, Oltvai ZN. Network biology: understanding the cell's functional organisation. Nat Rev Genet. 2004;5:101–113.
32. Deveraux QL, Reed JC. IAP family proteins — suppressors of apoptosis. Genes Dev. 1999;13:239–252.
33. Altieri DC. Survivin and IAP proteins in cell-death mechanisms. Biochem J. 2010;430:199–205.

 doi:10.20944/preprints202603.1918.v1

34. Fu P-Y, et al. New insight into BIRC3: a novel prognostic indicator and therapeutic target for liver cancer. J Cell Biochem. 2019;120:6035–6045.
35. Hou L, et al. UBE2D1 RNA expression is an independent unfavourable prognostic indicator in lung adenocarcinoma. Dis Markers. 2018:4108919.
36. He Y, et al. Interaction of EGFR with delta-catenin leads to delta-catenin phosphorylation and enhances EGFR signaling. Sci Rep. 2016;6:21207.
37. Huang F, et al. Hypoxia induces delta-catenin to enhance hepatocellular carcinoma progression via Wnt signaling. Exp Cell Res. 2019;374:94–103.
38. Anastasiadis PZ, et al. Inhibition of RhoA by p120 catenin. Nat Cell Biol. 2000;2:637–644.
39. Noren NK, et al. p120 catenin regulates the actin cytoskeleton via Rho family GTPases. J Cell Biol. 2000;150:567–580.
40. Vetter IR, Wittinghofer A. The guanine nucleotide-binding switch in three dimensions. Science. 2001;294:1299–1304.
41. Aguilar H, et al. VAV3 mediates resistance to breast cancer endocrine therapy. Breast Cancer Res. 2014;16:R53.
42. Tan B, et al. Inhibition of Vav3 reverses drug resistance in gastric cancer cells by downregulating JNK signaling. Cancer Gene Ther. 2014;21:526–531.
43. Dang TP, et al. Chromosome 19 translocation, overexpression of Notch3, and human lung cancer. J Natl Cancer Inst. 2000;92:1355–1357.
44. Wael H, et al. Notch1 signaling controls cell proliferation, apoptosis and differentiation in lung carcinoma. Lung Cancer. 2014;85:131–140.
45. Xie M, et al. Notch-1 contributes to EGFR-TKI acquired resistance in NSCLC in vitro and in vivo. Eur J Cancer. 2013;49:3559–3572.
46. Wang X, et al. miR-181b/Notch2 overcome chemoresistance by regulating cancer stem cell-like properties in NSCLC. Stem Cell Res Ther. 2018;9:327.
47. Gustafsson MV, et al. Hypoxia requires Notch signaling to maintain the undifferentiated cell state. Dev Cell. 2005;9:617–628.
48. Lu Y, et al. Hypoxia induces resistance to EGFR inhibitors in lung cancer via upregulation of FGFR1 and MAPK. Cancer Res. 2020;80:4655–4667.
49. Minakata K, et al. Hypoxia induces gefitinib resistance in NSCLC with mutant and wild-type EGFR. Cancer Sci. 2012;103:1946–1954.
50. Wei L, et al. Aberrant expression of HIF3A in plasma of patients with NSCLC and its clinical significance. J Clin Lab Anal. 2021;35:e23889.
51. Leclerc RD. Survival of the sparsest: robust gene networks are parsimonious. Mol Syst Biol. 2008;4:213.
52. Siegal ML, Bergman A. Waddington's canalization revisited: developmental stability and evolution. PNAS. 2002;99:10528–10532.
53. Menacho-Márquez M, et al. The Rho exchange factors Vav2 and Vav3 favour skin tumor initiation by engaging extracellular signaling loops. PLoS Biol. 2013;11:e1001615.